Modeling the Oxidative Degradation of Azo Dyes: A Density Functional Theory Study

ARTICLE *in* THE JOURNAL OF PHYSICAL CHEMISTRY A · MAY 2003

Impact Factor: 2.69 · DOI: 10.1021/jp026287z

2 AUTHORS, INCLUDING:

Viktorya Aviyente
Bogazici University
145 PUBLICATIONS **1,439** CITATIONS

SEE PROFILE

Modeling the Oxidative Degradation of Azo Dyes: A Density Functional Theory Study

Alimet S. Özen and Viktorya Aviyente*

Department of Chemistry, Bogazici University, 80815 Bebek-Istanbul, Turkey

Roger A. Klein

Institute for Physiological Chemistry, University of Bonn, D-53115 Bonn, Federal Republic of Germany

Received: June 12, 2002; In Final Form: February 24, 2003

In this paper, we show, using DFT methods, reactivity indices, and electron density topology, that oxidative degradation of azo dyes occurs through the cleavage of the N−N bond following hydroxyl radical addition to the chromophore. Structures for both experimentally proposed reaction pathways, involving either cleavage of the C−N or N−N bonds, have been optimized at the B3LYP/6-31G(d) level of theory; the energies were further refined using single point calculations at the B3LYP/6-311+G(d,p)//B3LYP/6-31G(d) level. Potential energy surfaces (PES) have been compared for the two mechanisms to determine which mechanism is energetically more favorable. Reactivity indices and electron density topology calculations confirmed the findings of the PES. Detailed electron density contour mapping allowed accurate visualization of the electron distribution, i.e., its topology, for the transition states. The effect of the medium dielectric constant was allowed for via self-consistent reaction field (SCRF) theory calculations using the IEFPCM method with water as solvent. A "super-molecule" approach involving complex formation between one solvent molecule and the molecules along the reaction pathway, was used to elucidate the mechanism of proton transfer.

Introduction

Azo dyes constitute a very large and important class of colorants, especially in the textile industry,[1−4] with the most important group consisting of aminobenzene derivatives of general formula[5]

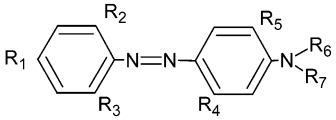

where R_1 is an electron-attracting group, R_2 and R_3 are H or an electron-attracting group, R_4 and R_5 are H or an electron-repelling group, and R_6 and R_7 are H or alkyl (often further substituted).

Oxidation of azo dyes by •OH radicals generated, for example, by chemical means, photochemical means, ultrasonic irradiation, or radiolysis using ionizing radiation, is important as a means of removing these pollutants, without the generation of potentially carcinogenic aromatic amines, from wastewater produced in the textile dyeing industry before it is discharged to the environment.[6,7] The most commonly used chemical process, known as Fenton's reaction, uses the reaction of ferrous or ferric salts with H_2O_2 to produce •OH:[6,8−12]

$$Fe^{2+} + H_2O_2 + H^+ \rightarrow Fe^{3+} + {}^{\bullet}OH + H_2O \qquad (1a)$$

$$Fe^{3+} + H_2O_2 \rightarrow Fe^{2+} + {}^{\bullet}OOH + H^+ \qquad (1b)$$

$$Fe^{3+} + {}^{\bullet}OOH \rightarrow Fe^{2+} + O_2 + H^+ \qquad (1c)$$

In photochemical oxidation •OH is produced using combinations such as UV/H_2O_2, UV/TiO_2, or UV/O_3.[13−18] Photocatalytic and photosensitized methods involve illumination of large-band gap semiconductor particles such as TiO_2, either dispersed as slurry in the contaminated wastewater or in the form of an immobilized film:[19−35]

$$OH^- + h(TiO_2) \rightarrow {}^{\bullet}OH \qquad (2a)$$

$$\text{dye} + {}^{\bullet}OH \rightarrow \text{products (environmentally safe substances)} \qquad (2b)$$

h being the positive holes on the catalyst surface.

In methods involving ultrasonic degradation, the irradiation produces cavitation in the liquid through which it is transmitted; collapse of the bubbles causes extreme conditions of heat and pressure locally. Under such conditions water is dissociated and chemically active species (radicals) are formed.[36−38]

Radiolytically generated radicals are very effective in degrading organic compounds. Free radicals are formed whenever water is irradiated with ionizing radiation such as γ-rays or high-energy electrons. The major reactive species generated are hydroxyl radicals and hydrated electrons (e_{aq}^-).[39−42] Two or three of these techniques may be used together to enhance degradation and to increase the degree of mineralization.[43−45]

Hydroxyl radicals can react with organic compounds by (i) hydrogen abstraction in the case of saturated organic compounds such as alcohols, (ii) addition to double bonds with unsaturated organic compounds such as aromatic rings, and (iii) one-electron oxidation, which is mostly nothing more than acid- or base-catalyzed loss of water from hydroxyl radical adducts with certain aromatic compounds.[14,40,46−48]

In the case of azo dyes, it is necessary to determine whether hydroxyl radical addition involves the −N═N− chromophore or the aromatic ring. Experimental studies[12,42,44,49] have shown that the main reaction pathway (∼60% of OH radicals[42]) is the addition of the hydroxyl radical to the double bond of the azo group, resulting in the rapid disappearance of color; however, addition to the aromatic ring also occurs (∼40% of OH radicals[42]). Although this bleaching reaction is very fast,

10.1021/jp026287z CCC: $25.00
Published on Web 05/28/2003

complete mineralization of the dye to yield small molecules, such as CO_2, NO_3^-, or SO_4^{2-}, takes much longer. The exact mechanism of the reaction is, however, not known. A key question is to determine whether it is the C atoms bearing the azo group, or the N═N− atoms themselves, that are attacked.

Using high-performance liquid chromatography (HPLC) and mass spectrometry (MS), two mechanisms (3) have been proposed for the oxidative cleavage reaction of azo dyes, involving either C—N or N—N cleavage:

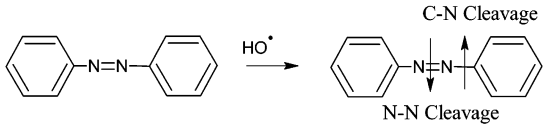

(3)

According to the mechanism proposed by Spadaro et al.,[6] a hydroxyl radical produced, for example, by Fenton's reaction, attacks the carbon atom bearing the azo linkage leading to the cleavage of the C—N bond and the generation of benzene.[7,9,11,13,19−21,24,39] On the other hand, Joseph et al., in their ultrasound study where •OH radical production was again enhanced with Fenton's reagent, proposed cleavage of the N—N bond, resulting in formation of nitrosobenzene.[26,37,42,44] Other authors have discussed azo-hydrazone tautomerism in ortho- or para-substituted azo compounds and its role in reaction 4:[10,18,50]

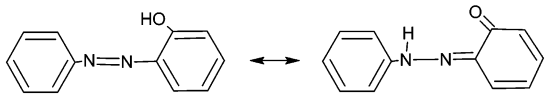

(4)

Experimental studies, which have managed to overcome the problems of dye purity and the trapping of short-lived intermediates successfully, point to plausible reaction pathways but without agreement on whether the C—N or N═N bond is attacked first, leading to quite different reaction mechanisms.

Theoretical calculations appear promising as a means of determining the reaction mechanisms for such complex reactions. The aim of this study is to model mechanisms proposed for the addition reactions of hydroxyl radicals to azo dyes using quantum mechanical molecular orbital calculations and to investigate the pathway that is energetically more preferred.

Theoretical Background

Density Functional Theory (DFT) and Open-Shell Systems.[51,52] The reaction system studied here consists of radicals, in other words, of open-shell molecules; it is known that "*open-shell molecules pose particular challenges for electronic structure methods*".[53] Wave function based UHF methods for open-shell systems suffer from spin-contamination[54] and generally do not give accurate results. Calculations at higher levels of theory are not "affordable", especially for large molecules, in terms of computational time and resources. On the other hand, density functional theory (DFT) methods[55,56] use the exact electron density instead of the wave function to calculate molecular properties, differing totally from traditional ab initio methods. Electron correlation, whose absence is the main drawback to HF methods, is accounted for in DFT methods that do not suffer from spin contamination, making them good candidates for calculations involving open-shell systems. DFT methods are also more efficient for large systems in terms of computer time compared to post-HF methods such as MP2.[53,54]

Choice of the basis set is very important to strike a compromise between computational time and accuracy. Wong et al.[57] have carried out a detailed study of radical addition to alkenes to determine the level of theory necessary for predicting reliable barriers heights. According to their results, B3LYP/6-31G(d) geometries and zero-point vibrational energies (ZPE) are preferable to both UHF and UMP2/6-31G(d) values. Calculations using B3LYP/6-311+G(d,p)//B3LYP/6-31G(d) are found to be more suitable for examining energy barriers for radical additions in large systems because, as found by Sekusak et al.,[58] B3LYP/6-31G(d) alone has a tendency to underestimate the barriers. According to Llano et al.,[59] who examined hydroxyl radical addition to imidazole, B3LYP/6-31G(d,p) geometry gives the same reactivity tendency as its MP2 counterpart, though it again results in lower activation barriers. Based on these findings, calculations reported in the present study use optimization at the B3LYP/6-31G(d) level followed by single point energy calculations at the B3LYP/6-311G+(d,p) level.

DFT-Based Reactivity Descriptors.[51,52] DFT methods may not only be used to calculate molecular properties, potential energy surfaces, and the course of a given reaction but are also very useful tools for obtaining conceptual information about chemical reactivity, as well as for treating qualitative concepts such as hardness and electronegativity.[55,56,60−93] Because the electron density is considered to contain all the information about molecular properties, chemical reactivity should be reflected in its sensitivity to perturbation.[76] Moreover, the distribution of the electron density between the nuclear attractors is particularly informative in understanding the structure of the transition states. If electronic energy is defined as a function of the number of electrons and external potential, $E\,[N, v(r)]$, these perturbations can be obtained by a series of derivatives of the energy. Perturbations due to changes in the number of electrons are defined as "global" properties[76] and are related to overall molecular stability. Perturbations due to changes in external potential are classified as "local" properties[76] and determine the site selectivity of a molecule for a specific reaction type. Indices of local chemical reactivity obtained from density functional theory may be defined in the form of Fukui functions as follows.

The Fukui function is a space-dependent local function and "*it measures how sensitive a system's chemical potential is to an external perturbation at a particular point*".[55] It also gives information about a quantity related to the electron density of an atom or molecule in its frontier regions:[55,69]

$$f(r) = \delta\mu/\delta v(r) = \delta\rho(r)/\delta N \tag{5}$$

Because, however, $\delta\rho(r)/\delta N$ is a discontinuous function of N, it will have one value from the right, one from the left, and an average at some integral value of N:

$$f^+(r) = [\delta\rho(r)/\delta N]^+ \qquad (\text{as } N \text{ goes from } N_0 \text{ to } N_0 + \delta) \tag{6a}$$

$$f^-(r) = [\delta\rho(r)/\delta N]^- \qquad (\text{as } N \text{ goes from } N_0 - \delta \text{ to } N_0) \tag{6b}$$

$$f^0(r) = {}^1/_2[f^+(r) + f^-(r)]^0 \qquad (\text{average}) \tag{6c}$$

Here $f^+(r)$ is the reactivity index for a nucleophilic attack, $f^-(r)$ for an electrophilic attack, and $f^0(r)$ for a radical attack. Within the finite difference approximation, these relationships can be written as

$$f^+(r) = \delta\rho_N(r) - \delta\rho_{N-1}(r) \tag{7a}$$

$$f^-(r) = \delta\rho_{N+1}(r) - \delta\rho_N(r) \tag{7b}$$

$$f^0(r) = {}^1/_2[\delta\rho_{N+1}(r) - \delta\rho_{N-1}(r)] \quad (7c)$$

A condensed form of these functions employs the atomic charges:[61]

$$f^+ = q_k(N+1) - q_k(N) \quad (8a)$$

$$f^- = q_k(N) - q_k(N-1) \quad (8b)$$

$$f^0 = {}^1/_2[q_k(N+1) - q_k(N-1)] \quad (8c)$$

Methodology

Gaussian98 has been employed for the calculation of geometries and energies.[94] Optimizations were performed at the B3LYP/6-31G(d) level of theory. Ground state and transition state structures have been confirmed by frequency analyses at the same level. Transition structures have been characterized by having one imaginary frequency that belonged to the reaction coordinate, corresponding to a first-order saddle point. Zero point vibrational energies (ZPEs) were calculated at the B3LYP/6-31G(d) level; these were not scaled because they were only used for comparing possible reaction mechanisms. The same ZPEs were used for the B3LYP/6-311+G(d,p)//B3LYP/6-31G(d) calculations. Solvent effects were modeled using the integral equation formalism (IEF) polarized continuum model (PCM) of Tomasi et al.[95] within self-consistent reaction field (SCRF) theory, by means of single-point calculations based on the gas-phase geometries. Electronic populations for the calculation of Fukui indices were obtained from Mulliken population analysis and natural population analysis.

Wave function files were generated within Gaussian98 using the (output=wfn) option and Cartesian coordinates (6D 10F), before being analyzed for the electron density contours and topological critical points using the AIM2000 implementation of Bader's AIMPAC suite of programs (Biegler-König et al.[96]).

Results and Discussion

Experimental and Theoretical Model Reaction Mechanisms. *C−N Bond Cleavage Mechanism.* The mechanism involving cleavage of the C−N bond was first proposed by Spadaro et al.,[6] who investigated the degradation of ^{14}C-labeled azo dyes by hydroxyl radicals produced from Fe^{2+} and H_2O_2 and concluded that the initial attack by •OH radicals occurred at the C atom bearing the azo linkage. Their main concern was the generation of benzene as a pollutant resulting from the oxidation reaction. Other findings support this mechanism.[6,9,11,13,19−21,24,39]

Scheme 1 represents the potential energy profile of the DFT-modeled mechanism for the C−N bond cleavage pathway of azobenzene (**1**) (Figure 1)in the gas phase and also in water. In this mechanism, attack by OH radicals at the C atom next to the azo linkage leads to a transition state (**TS(1-2C)**) in which the −O···C− distance is 1.964 Å (no precomplex structure was found in IRC calculations). As a result of the stability of the resonance ring structure (**2C**), the C−N bond breaks (**TS(2C-3C,4C)**), leading to the formation of a phenyldiazene radical (**3C**) and a phenol molecule (**4C**), followed by cleavage to give a phenyl radical and molecular nitrogen. The former can be reduced to benzene. Solvent has a stabilizing effect in terms of the overall energy along the C−N cleavage pathway, but the barriers in solution are slightly higher, relatively, than the barriers in vacuo by 0.9−1.4 kcal/mol.

SCHEME 1: Potential Energy Profile along the C−N Bond Cleavage Pathway[a]

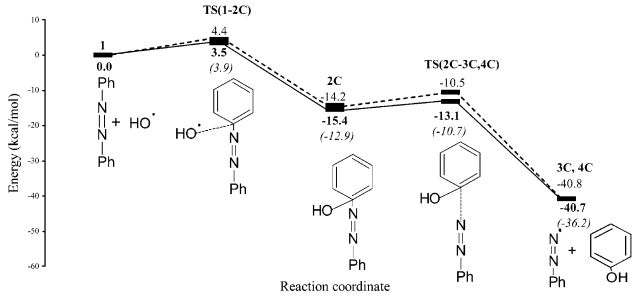

Key: (−) relative energies obtained at B3LYP/6-31G(d) (bold) and B3LYP/6-311+G(d,p)//B3LYP/6-31G(d) (in parentheses) levels of theory with ZPE corrections at B3LYP/6-31G(d); (---) solvent effects from IEFPCM calculations at the B3LYP/6-31G(d) level of theory (dashed lines). 0.0 kcal/mol on the relative energy axis corresponds to **1** + •OH = −648.285865 (*−648.470485*) hartrees at B3LYP/6-31G(d) (B3LYP/6-311+G(d,p)//B3LYP/6-31G(d)) and **1** + •OH = −648.501393 hartrees in IEFPCM.

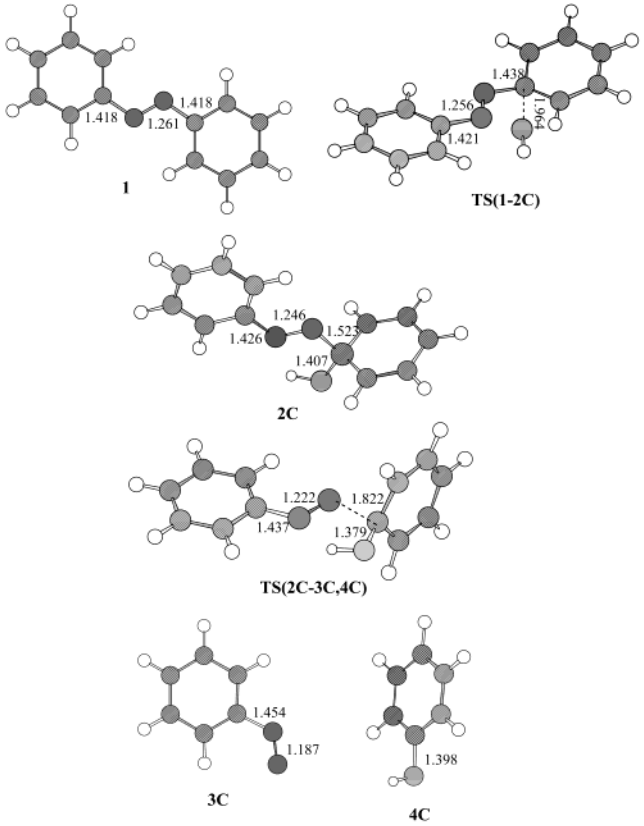

Figure 1. Optimized geometries for the C−N cleavage pathway.

Electron Density Topological Analysis of the C−N Cleavage Transition States. The electron density topology of the transition state structure **TS(1-2C)** in Scheme 1 is shown in Figure 2. Electron density contours are drawn at 0.001, 0.002, 0.004, 0.008, 0.020, 0.040, ... au; bond critical points (BCPs) are shown by small dots, and ring critical points (RCPs), by crosses. This transition state is characterized by an atomic bond path with a bond critical point (BCP) of (3, −1) topology between the oxygen atom of the OH radical and C1 of the aromatic ring. The value for the electron density at the BCP of 0.07531 au is associated with a positive Laplacian of ρ, $\nabla^2(D)$, of +0.14643 au, indicating local depletion of electronic charge at the BCP and a local excess in electronic kinetic energy (Bader[97]). The bond electronic interaction energy, based on $G(r)$ and $\nabla^2(D)$ as

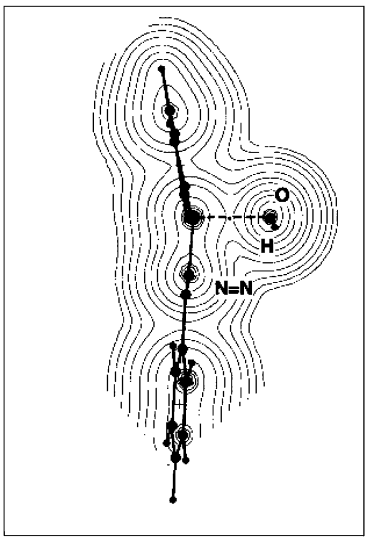

Figure 2. Transition state **TS(1-2C)**. Electron density contours, almost through the plane of the two aromatic rings and the azo −N═N− group, are shown at 0.001, 0.002, 0.004, 0.008, 0.020, 0.040, ... au (used as default); (3, −1) bond critical points (BCPs) are shown as small dots, (3, +1) ring critical points (RCPs) as crosses. Covalent bonds are shown as heavy lines.

described by Espinosa and Molins,[98] amounts to 19.2 kcal/mol. The electron density topology, shown for a slice through the interacting nuclei in Figure 2, is typical for a fairly strong closed shell interaction.

N−N Bond Cleavage Mechanism. Intermediate and end-product analysis, as part of ultrasonic cleavage studies in which the Fenton reaction ($Fe^{2+} + H_2O_2$) was used to enhance •OH reactivity in the reaction between azo dye and the hydroxyl radical, has provided evidence for nitrophenyl (NO_x) compounds and thus a mechanism by which the azo linkage is broken.[44] Scheme 2 represents the potential energy profile of the DFT-modeled mechanism for the first stages of the N−N bond cleavage pathway for azobenzene (**1**) (Figure 3)in the gas phase and also in solution. A prereaction complex (**2N**) is observed as the OH radical approaches the azobenzene molecule with an −O···N− distance of 2.4 Å; formation of the transition state structure (**TS(2N-3N)**) reduces this distance to 1.91 Å. In the intermediate radical (**3N**), the bond distance for the newly formed bond is 1.44 Å, in good agreement with the value for a single N−O bond. This radical is mentioned in Patai's book on azo compounds,[99] as undergoing the following cleavage reaction:

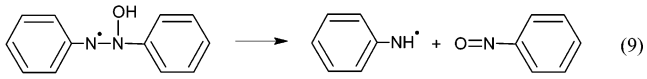

(9)

The reaction probably proceeds through the protonation of the neighboring nitrogen atom and cleavage of the N−N bond. Thus the H atom of the OH group approaches the neighboring N atom, forming a cyclic transition state structure (**TS(3N-4N)**). As the N−H bond forms, the O−H bond is broken leading to another radical intermediate (**4N**). To obtain resonance stabilization, the oxygen atom forms a double bond with the nitrogen to which it is attached, abstracting in resonance stabilization and abstracting an electron from the bond between two nitrogen atoms. Weakening of the former −N═N− linkage results in cleavage of the dye molecule into the phenylamine radical (**5N**) and nitrosobenzene (**6N**) via the transition state (**TS(4N-5N,6N)**).

The presence of a dielectric medium has a stabilizing effect, decreasing the overall energy for this mechanism as in the case with C−N cleavage mechanism. Because, however, this reduction in energy is more for the ground state molecules (the initial radical-attack complex being an exception) and relatively less for transition state molecules, the barrier heights increase. This effect is most pronounced for the proton-transfer barrier, which increases from 24 to 31.5 kcal/mol.

Electron Density Topological Analysis of the N−N Cleavage Transition States. The electron density topology of the transition state structures **TS(2N-3N)** and **TS(3N-4N)** in Scheme 2 are shown in Figures 4a,b and 5. The transition state **TS(2N-3N)** is characterized by the oxygen of the OH radical being hydrogen-bonded to two activated sp^2 hydrogen atoms, each at the ortho position on each of the separate aromatic rings. The electron density contours, shown for two offset planes in Figure 4a,b, illustrate clearly the topological features of this transition state, namely, the three (3, −1) bond critical points associated with two (3, +1) ring critical points, thus satisfying the Poincaré−Hopf relationship. The electron densities and positive

SCHEME 2: Potential Energy Profile along the C−N Bond Cleavage Pathway[a]

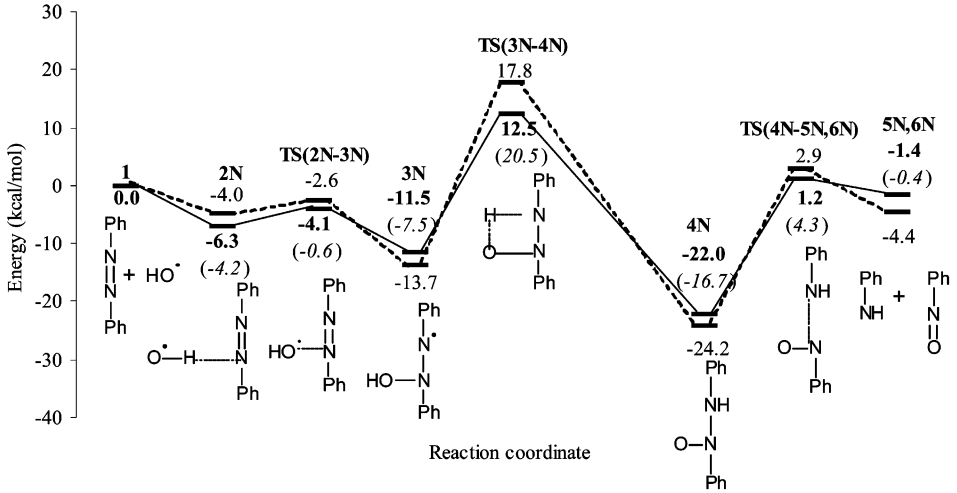

Key: (—) relative energies obtained at B3LYP/6-31G(d) (bold) and B3LYP/6-311+G(d,p)//B3LYP/6-31G(d) (italic in parentheses) levels of theory with ZPE corrections at B3LYP/6-31G(d); (---) solvent effects from IEFPCM calculations at the B3LYP/6-31G(d) level of theory (dashed lines). 0.0 kcal/mol on the relative energy axis corresponds to **1** + •OH = −648.285865 (*−648.470485*) hartrees at B3LYP/6-31G* (B3LYP/6-311+G(d,p)//B3LYP/6-31G(d)) and **1** + •OH = −648.501393 hartrees in IEFPCM.

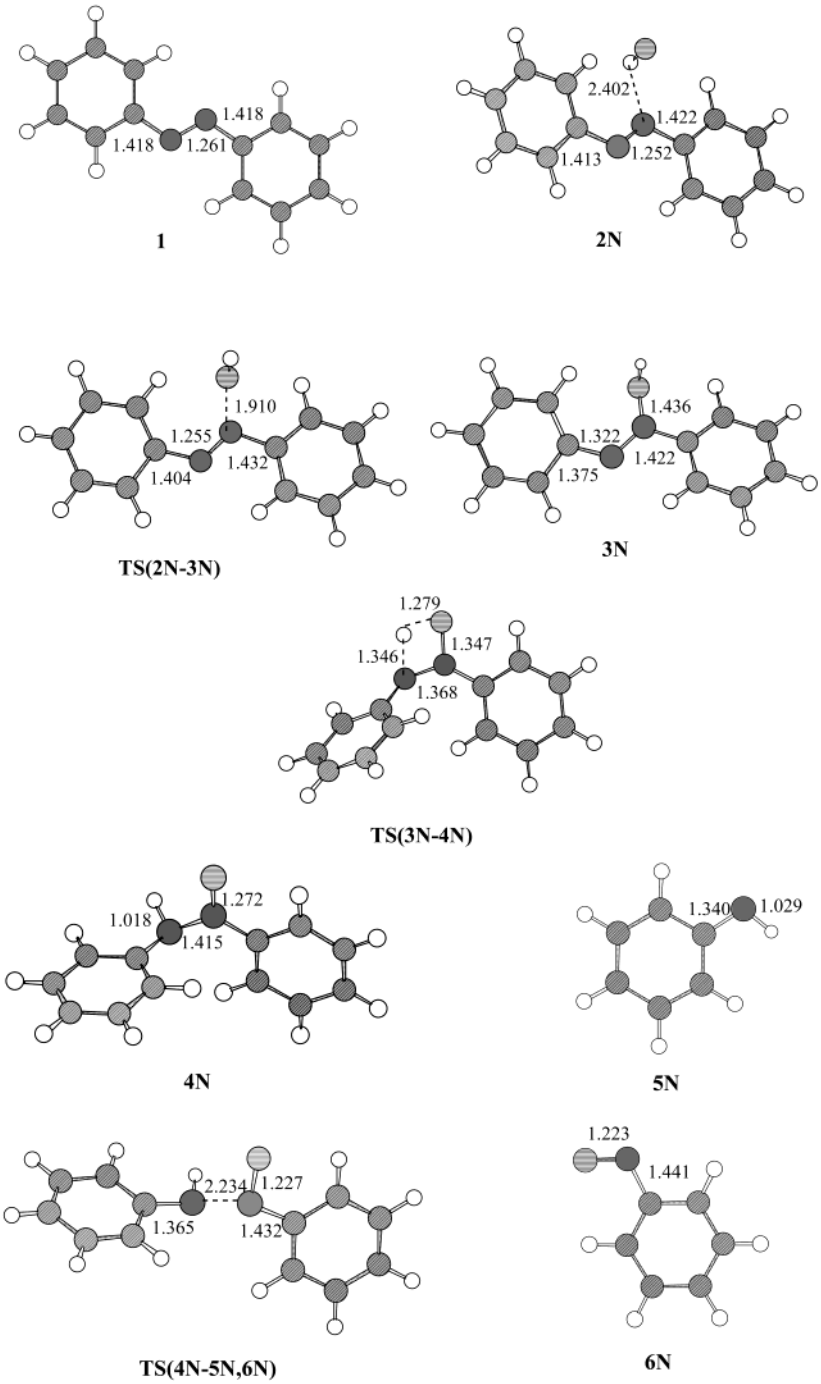

Figure 3. Optimized geometries for the N−N cleavage pathway.

Laplacian of ρ at the (3, −1) BCPs, as well as the electronic interaction energies, are typical for weak hydrogen bonds: $\rho = 0.01838$ and 0.02088 au, $\nabla^2(\rho) = +0.06535$ and $+0.06538$ au, respectively; interaction energies are 4.5 and 5.3 kcal/mol. The free radical oxygen atom also shows an atomic bond path to the nitrogen atom of the azo −N═N− group with an electron density at the (3, −1) BCP of 0.09137 au, $\nabla^2(\rho) = +0.26748$ au, and a calculated interaction energy of 25.5 kcal/mol. Ring critical points (RCPs) are present for the two ring systems generated by this bonding pattern, as shown in Figure 4a,b.

The transition state **TS(3N-4N)**, shown in Figure 5, demonstrates rotation of both aromatic rings so that the ortho hydrogens no longer interact with the free radical oxygen atom. Instead, the oxygen−nitrogen bond becomes shorter (1.347 Å), comparable to a covalent N−O bond, with increased electron density and a negative Laplacian of ρ at the BCP, 0.37297 and −0.56264 au, respectively, indicating concentration of electronic charge with the potential energy dominating both the local total electronic energy $E_e(r)$ and the local virial relationship,[97] typical of a covalent closed-shell interaction. The estimated electronic interaction energy is very high, namely, 196.7 kcal/mol.

The free radical hydrogen atom becomes placed more or less symmetrically between the oxygen atom and the second nitrogen atom of the azo −N═N− group, i.e., the one not bonded to the oxygen atom, with an atomic bond path linking it to both oxygen and nitrogen atoms. The electron density and Laplacian of ρ, at the two BCPs are $\rho = 0.14468$ au, $\nabla^2(\rho) = -0.09419$ au (1.279 Å) and $\rho = 0.12982$ au, $\nabla^2(\rho) = -0.04735$ au (1.346 Å), corresponding to interaction energies of 56.2 and 43.3 kcal/

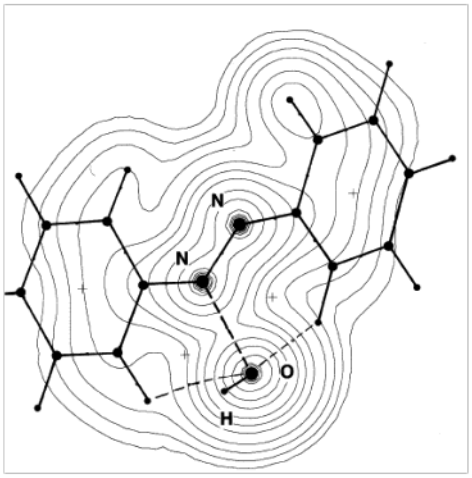

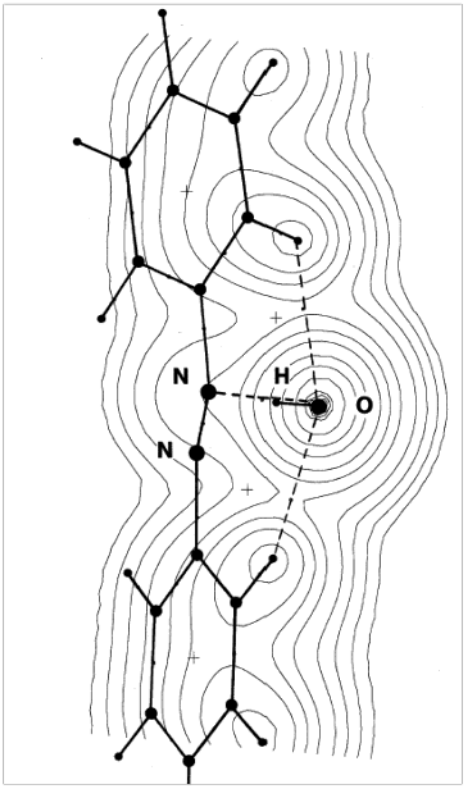

Figure 4. (a) Transition state **TS(2N-3N)**. Electron density contours are shown through the plane of the OH radical oxygen atom and the two azo notrogen atoms. Hydrogen bonding of the oxygen atom to the two aromatic ortho hydrogen atoms is shown as a light broken line. (b) Transition state **TS(2N-3N)**. Electron density contours are shown through the plane of the OH radical oxygen atom and the two aromatic ortho hydrogen atoms, demonstrating the BCPs for the two hydrogen bonds formed.

mol, respectively. Both Laplacians are negative, indicating concentration of electronic charge at the BCP. There is a clear RCP for this strained four-membered ring consisting of the O—N—N—H atoms. The topological analysis, as well as the representative slice through the electron density distribution giving the contours shown in Figure 5, highlights the predominantly covalent, shared interaction in this tight transition state, with the hydrogen atom poised almost equidistant from the donor oxygen and acceptor nitrogen atoms (donor and acceptor on this occasion in the sense of the reaction coordinate). Analysis of the infrared spectrum shows oscillation of the hydrogen atom across this first-order saddle point, as the O—H bond in structure

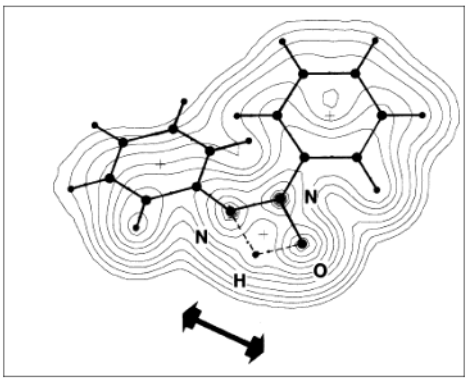

Figure 5. Transition state **TS(3N-4N)**. Electron density contours are shown through the plane of the OH radical oxygen atom and the two azo nitrogen atoms, demonstrating the strong hydrogen bonds between the radical hydrogen atom and the oxygen and nitrogen atoms. The double-headed arrow refers to the IR frequency corresponding to the first-order saddle point.

3N is broken and the N—H bond in structure **4N** formed. These two hydrogen−oxygen interactions would be classified as very strong, short hydrogen bonds with considerable covalent character, in particular with a negative Laplacian of ρ at the BCP although not as high as for a standard covalent bond.

Water-Assisted Mechanism for Both Pathways: Supermolecule Approach. When the potential energy surfaces for the two reactive pathways for the initial attack are compared, the N−N cleavage path is lower in energy and the C−N cleavage pathway is endothermic. The high-energy intermediate proton transfer in the former mechanism is, therefore, of great interest for the later stages of the reaction.

Because these reactions actually take place in water, water molecules surrounding the molecule in the first solvation shell may be involved. Indeed, the presence of a water molecule hydrogen-bonded to one of the nitrogen atoms has been found to lower the energy of proton transfer to a large extent through a subsequent cyclic rotational transition state due to the cooperative hydrogen bonding for the N−N cleavage pathway. For the sake of consistency, a water molecule has been added to all the molecules in both pathways using optimization at the same level of theory.

It must be noted that the attempt is neither to define the hydrogen bonding in the first solvation shell nor to perform a discrete solvent survey of the complete supermolecule-type approach, because this would require statistical mechanical calculations, e.g., Monte Carlo or Car−Parinnello type calculations, for the proper location of the water molecules. Actually, the water molecule that assists the reaction can be anywhere around the azobenzene molecule but when it is hydrogen bonded to an N atom, it assists the proton transfer. These structures have been calculated in a polarized continuum (PCM) model with water as solvent to simulate the experiments.

Water-Assisted C−N Bond Cleavage Mechanism. Scheme 3 represents the potential energy profile of the DFT-modeled mechanism for the C−N bond cleavage pathway of the azobenzene−water complex (**1W**) (Figure 6) in the gas phase and also in water as solvent. The presence of water leads to a prereactive complex through hydrogen bonding between the free H atom of water molecule and O atom of OH radical, which is not observed in the C−N cleavage mechanism without water present. The strength of this hydrogen bond is reduced by the approach of OH radical and the bond distance increases from 1.997 to 2.251 Å. After addition of the radical is complete, a new hydrogen bond is formed between the hydrogen atom of

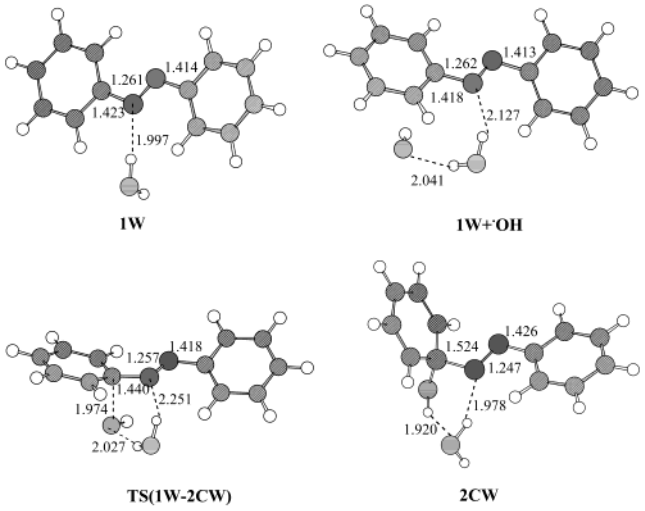

Figure 6. Optimized geometries for the water assisted C−N cleavage pathway.

SCHEME 3: Potential Energy Profile along the Water-Assisted C−N Bond Cleavage Pathway[a]

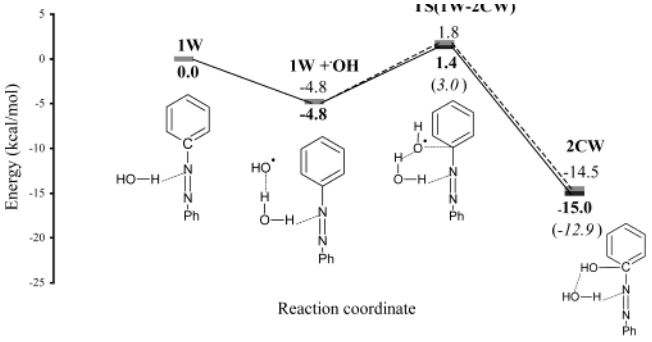

Key: (—) relative energies obtained at B3LYP/6-31G(d) (bold) and B3LYP/6-311+G(d,p)//B3LYP/6-31G(d) (italic in parentheses) levels of theory with ZPE corrections of B3LYP/6-31G(d); (---) solvent effect from IEFPCM calculations at the B3LYP/6-31G(d) level of theory (dashed lines). 0.0 kcal/mol on the relative energy axis corresponds to **1W** + •OH = −724.683860 (*−724.910761*) hartrees at B3LYP/6-31G* (B3LYP/6-311+G(d,p)//B3LYP/6-31G(d)) and **1W** + •OH = −724.923981 hartrees in IEFPCM.

the OH and the oxygen atom of the water molecule, which is stronger than the former one (1.978 Å). Use of a dielectric medium decreases the overall reaction energy but has a negligible effect on the barrier heights.

Water-Assisted N−N Bond Cleavage Mechanism. Scheme 4 represents the potential energy profile of the DFT-modeled mechanism for the N−N bond cleavage pathway of the azobenzene−water complex (**1W**) (Figure 7) in the gas phase and also in water. As in the case with the C−N cleavage mechanism, addition of the OH radical decreases the strength of the hydrogen bond between water and azobenzene, but by a smaller degree (**2NW**, **TS(2NW-3NW)**). There is no hydrogen bonding between the water molecule and the OH radical because the radical approaches from the other side and forms a complex (**2NW**) with the other N atom through its hydrogen atom. Water interacts with the OH radical only after rotation around the N−N bond and its oxygen atom forms a strong hydrogen bond with the hydrogen atom of the OH group (**TS(3NW-4N**). It releases the hydrogen atom, and the nitrogen atom of the azo linkage captures the proton. It is as if the proton were transferred via a water-bridge transition state. The presence of a dielectric medium affects this pathway more than its counterpart, increasing the barrier heights.

SCHEME 4: Potential Energy Profile along the Water-Assisted N−N Bond Cleavage Pathway[a]

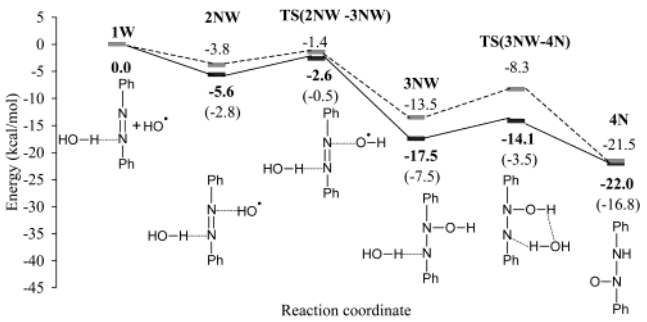

Key: (—) relative energies obtained at B3LYP/6-31G(d) (bold) and B3LYP/6-311+G(d,p)//B3LYP/6-31G(d) (italic in parentheses) levels of theory with ZPE corrections of B3LYP/6-31G(d); (---) solvent effects from IEFPCM calculations at the B3LYP/6-31G(d) level of theory (dashed lines). 0.0 kcal/mol on the relative energy axis corresponds to **1** + •OH = −724.683860 (*−724.910761*) hartrees at B3LYP/6-31G* (B3LYP/6-311+G(d,p)//B3LYP/6-31G(d)) and **1** + •OH = −724.923981 hartrees in IEFPCM.

Comparison of the Energy Barriers for the Two Proposed Mechanisms. To determine the most probable mechanism from among those proposed on the basis of experimental evidence, potential energy surfaces were compared (Schemes 1 and 2). The main difference between the two proposed mechanisms is that the initial radical-attack transition-state that proceeds through a prereactive complex is lower in energy than the reactants for the N−N bond cleavage pathway, whereas in the case of C−N cleavage the transition-state for the initial attack is of higher energy than the reactants and no prereactive complex was observed using IRC calculations.

The energy difference between the two initial attack transition states, ΔE [**TS(1-2C)** − **TS(2N-3N)**], is 7.6 and 7.0 kcal/mol in vacuo and in water, respectively. Additionally, the effect of using a dielectric medium is more pronounced for the N-attack pathway than for the C-attack pathway. This effect is minimal in the case of the C-attack pathway supermolecule.

The energy gap between the initial attack transition states is reduced by the addition of an extra water molecule, due to hydrogen bonding (ΔE[**TS(1W-2CW)** − **TS(2NW-3NW)**] = 4.0 kcal/mol for the gas phase and 3.2 kcal/mol in water), but it is never overcome completely (Schemes 3 and 4).

Increasing the size of the basis set decreases the gap between the two competing transition-states but still retains a substantial difference in energy (ΔE) and so one is able to differentiate between the most probable site of attack: ΔE [**TS(1-2C)** − **TS(2N-3N)**] is 4.5 kcal/mol in vacuo and 3.5 kcal/mol for the water-assisted mechanisms at the 6-311+G(d,p)// 6-31G(d) level of theory.

An Experimental Comment

A very interesting conclusion has been reached through detailed examination of a range of published data.[6,7,9−11,13,18−24,26,28,37,39,42,43] The experiments pointing to cleavage of the C−N bond were performed under conditions that support the formation of a hydrazone tautomer for the N═N compound, i.e., azo dyes with ortho- and/or para-OH or $-NH_2$ substituents in acidic media or polar solvents; it is possible, therefore, that a hydrazone tautomer is the reactant species rather than an azo tautomer under these conditions. Thus, also on the basis of our calculations, azo compounds would be cleaved through the N═N bond in their reaction with OH radicals unless conditions favor the formation of a hydrazone tautomer, in which

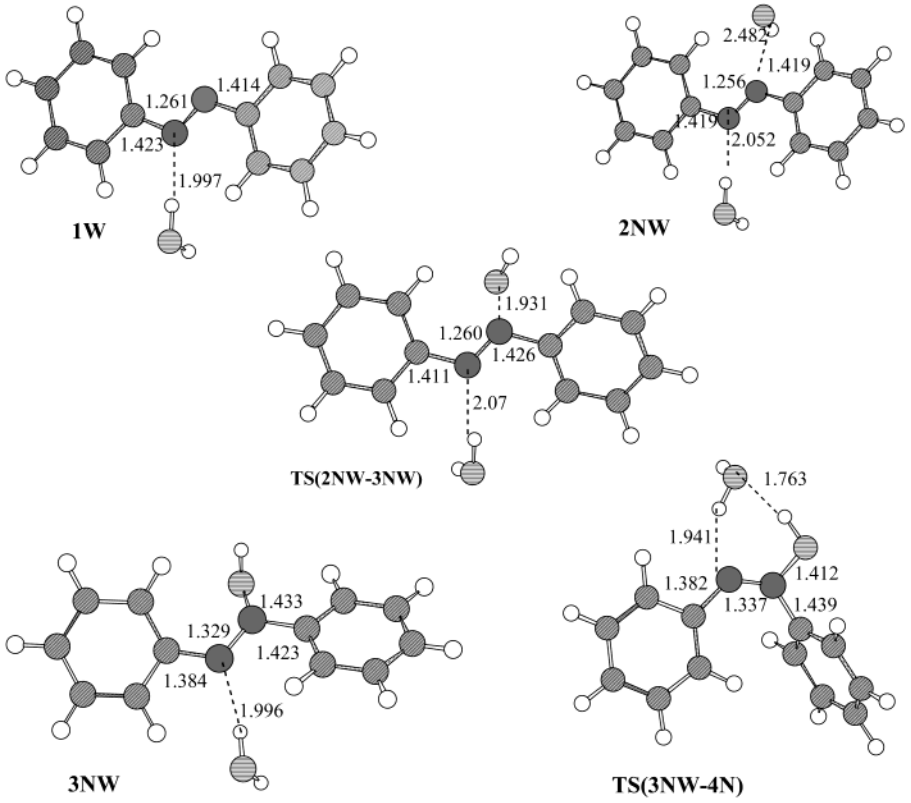

Figure 7. Optimized geometries for the water-assisted N−N cleavage pathway.

TABLE 1: Condensed Fukui Functions for the Radical Addition to Azobenzene

atomic center	Mulliken	NPA
C (**1**)	0.00755	−0.02716
N (**1**)	0.12405	0.20684
C (**1** in solution)	0.01893	−0.01515
N (**1** in solution)	0.15912	0.24062
C_1 (**1W**)	0.01039	0.02498
N_2 (**1W**)	0.06528	0.09824
N_3 (**1W**)	0.06777	0.09680
C_4 (**1W**)	0.01760	0.02454

case a different mechanism will be operative, leading to cleavage of the C−N bond. Also, with regard to the experimental findings with fast bleaching, i.e., rapid disappearance of color and with slow mineralization and degradation to small molecules, the evidence points to a mechanism controlled kinetically in the early stages but controlled thermodynamically at a late stage. This experimental observation is paralleled by the N−N cleavage mechanism with a fast initial attack followed by a slower bond-cleavage step.

To obtain a better insight into the choice of the attack-site, DFT concepts of chemical reactivity, such as condensed Fukui indices have been employed.

Site Selectivity

Condensed Fukui Indices for Radical Reactions. Fukui indices, representing local reactivity indices determining the site selectivity of a given reaction, are given in Table 1 only for the most susceptible sites for radical addition in azobenzene (**1**) in both the gas phase and in solution, and for radical addition to the supermolecule (**1W**) in the gas phase.

A more positive value for the condensed Fukui index implies greater susceptibility for certain types of reaction. The N atom seems, therefore, to be the preferred site for the concerted addition reaction involving OH radical attack compared to the C atom, for the two population analysis techniques used, confirming the findings based on our energy calculations.

In an attempt to understand the effect of dielectric medium on the initial attack, Fukui functions have been considered as a function of the dielectric constant ϵ, because the energy of the system is itself a function of dielectric constant.[100] To achieve this, azobenzene was fully optimized in water using the IEFPCM model. When the Fukui functions are compared for N and C, it is clear that the nitrogen atom is the most susceptible site for a radical attack in solvent too. Radical Fukui functions for the azobenzene−water complex (**1W**) are given in Table 1, using the following numbering system:

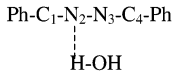

Again, the nitrogen atoms appear to be the most susceptible site for the radical attack.

It should be noted, moreover, that Mulliken population analysis is adequate in giving comparable results to the energy calculations.

Conclusions

The purpose of this study was to determine the preferred reaction mechanism, from among pathways that had been proposed on the basis of experimental evidence in the literature, for the OH radical addition reaction to azobenzene as the simplest representative of the azodyes and thus to model the advanced oxidation reactions of azo dyes. Topological analysis of the electron density, using the AIM approach formulated by R. F. W. Bader, has provided important insights into the structure of the various transition states involved

Comparison of the potential energy surfaces and application of local reactivity indices points to a reaction mechanism in which the N−N bond is broken in preference to the C−N bond being broken. The rapid disappearance of color in dye solutions, as well as the fact that mineralization is found to be the rate-determining step experimentally, is reflected by the N═N cleavage mechanism. Moreover, it seems most probable that the presence of the hydrazone tautomer in experimental studies, rather than the azo tautomer, resulted in the proposed reaction mechanism involving C−N bond cleavage.

Acknowledgment. We thank Boğaziçi Üniversitesi Bilimsel Araştırma Projeleri (BAP 02B501) and Devlet Planlama Teşkilatı (DPT 98K 120900) for financial support. The visit of R.A.K. to Boğaziçi Üniversitesi was supported by TÜBİTAK "Konuk Bilim Adamı Destekleme Programı". R.A.K. also acknowledges continued financial support in the form of a program grant (SFB 284/A1) from the Deutsche Forschungsgemeinschaft. Fruitful discussions with Prof. Nilsun İnce and Gökçe Tezcanlı from the Institute of Environmental Sciences, Bogazici University, are gratefully acknowledged.

References and Notes

(1) Correia, V.; Stephenson, T.; Judd, J. *Environ. Technol.* **1994**, *15*, 917−929.

(2) U. S. environmental Protection Agency. *Best Management Practices For The Pollution Prevention In The Textile Industry*; Center For Environmental Research Information: Cincinnati, OH, 1995.

(3) Whaley, W. M. Dyes Based On Safer Intermediates. Unpublished Paper presented at NC State University Fiber and Polymer Science Seminar Series, 1984.

(4) Reife, A., Freeman, H. S., Eds.; *Environmental Chemistry of Dyes and Pigments*; John Wiley and Sons Inc.: New York, 1996.

(5) Stevens, C. B. (I) Dye Classes: General Structure and Properties in Relation to Use. In *The Dyeing of Synthetic Polymer and Acetate Fibres*; Nunn, D. M., Ed.; Dyers Company Publications Trust: Bradford, 1979; p 1.

(6) Spadaro, J. T.; Isabelle, L.; Renganathan, V. *Environ Sci. Technol*. **1994**, *28*, 1389−1393.

(7) Vinodgopal, K.; Kamat, P. V. In *Environmental Applications of Ionizing Radiation*; Cooper, W. J., Curry, R. D., O'Shea, K. E., Eds.; John Wiley & Sons: New York, 1998; pp 587−599.

(8) Kuo, W. G. *Water Res.* **1992**, *26*, 881−886.

(9) Nam, S.; Renganathan, V.; Tratnyek, P. G. *Chemosphere* **2001**, *45*, 59−65.

(10) MacKay, A. A.; Pignatello, J. J. *Helv. Chim. Acta* **2001**, *84*, 2589−2600.

(11) Bandara, J.; Nadtochenko, V.; Kiwi, J.; Pulgarin, C. *Water Sci. Technol.* **1997**, *35* (4), 87−93.

(12) Tang, W. Z.; Chen, R. Z. *Chemosphere* **1996**, *32* (5), 947−958.

(13) Galindo, C.; Jacques, P.; Kalt, A. *J. Photochem. Photobiol. A: Chem.* **2000**, *130*, 35−47.

(14) Colonna, G. M.; Caronna, T.; Marcandalli, B. *Dyes Pigments* **1999**, 211−230.

(15) Shu, H. Y.; Huang, C. R.; Chang, M. C. *Chemosphere* **1994**, *29* (12), 2597−2607.

(16) Ince, H. N.; Stefan, M. I.; Bolton, J. R. *J. Adv. Oxid. Technol.* **1997**, *2* (3), 442−448.

(17) Imamura, K.; Hiramatsu, A.; Imada, M.; Sakiyama, T.; Tanaka, A.; Yamada, Y.; Nakanishi, K. *J. Chem. Eng. Jpn.* **2000**, *33* (2), 253−261.

(18) Galindo, C.; Jacques, P.; Kalt, A. *J. Adv. Oxid. Technol.* **1999**, *4* (4), 400−407.

(19) Poulios, I.; Aetopoulou, I. *Environ. Technol.* **1999**, *20*, 479−487.

(20) Hustert, K.; Zepp, R. G. *Chemosphere* **1992**, *24*, 335−342.

(21) Tanaka, K.; Padermpole, K.; Hisanaga, T. *Water Res*. **2000**, *34* (1), 327−333.

(22) Dieckmann, M. S.; Gray, K. A. *Chemosphere* **1994**, *28* (5), 1021−1034.

(23) Vinodgopal, K.; Wynkoop, D. E.; Kamat, P. V. *Environ. Sci. Technol*. **1996**, *30*, 660−666.

(24) Nasr, C.; Vinodgopal, K.; Fisher, L.; Hotchandani, S.; Chattopadhyay, A. K.; Kamat, P. V. *J. Phys. Chem.* **1996**, *100*, 8436−8442.

(25) Turchi, C. S.; Ollis, D. F. *J. Catal.* **1990**, *122*, 178−192.

(26) Devi, L. G.; Krishnaiah, G. M. *J. Photochem. Photobiol. A: Chem.* **1999**, *121*, 141−145.

(27) Gonçaives, M. S. T.; Oliveira-Campos, A. M. F.; Pinto, E. M. M. S.; Plasencia, P. M. S. *Chemosphere* **1999**, *39* (5), 781−786.

(28) Bauer, C.; Jacques, P.; Kalt, A. *J. Photochem. Photobiol. A: Chem.* **2001**, *140*, 87−92.

(29) Tang, W. Z.; Zhang, Z.; An, H.; Quintana, M. O.; Torres, D. F. *Environ. Technol.* **1997**, *18*, 1−12.

(30) Fox, M. A.; Dulay, M. *Chem. Rev.* **1993**, *93*, 341−357.

(31) Matthews, R. W. *Water Res*. **1991**, *25* (10), 1169−1176.

(32) Ruan, S.; Wu, F.; Zhang, T.; Gao, W.; Xu, B.; Zhao, M. *Mater. Chem. Phys.* **2001**, *69*, 7−9.

(33) Arslan, I.; Balcioglu, I. A. *Dyes Pigments* **1999**, 95−108.

(34) Chun, H.; Yizhong, W. *Chemosphere* **1999**, *39* (12), 2107−2115.

(35) Arslan, I.; Balcioglu, I. A.; Bahnemann, D. W. *Dyes Pigments* **2000**, *47*, 207−218.

(36) Ince, N. H.; Tezcanli, G.; Belen, R. K.; Apikyan, I. G. *Appl. Catal. B: Environ.* **2000**, *766*, 1−10.

(37) Destaillats, H.; Turjanski, A. G.; Estrin, D. A.; Hoffmann, M. R. *J. Phys. Org. Chem*. **2002**, *15*, 287−292.

(38) Vinodgopal, K.; Peller, J.; Makogon, O.; Kamat, P. V. *Water Res*. **1998**, *32* (12), 3646−3650.

(39) Das, S.; Kamat, P. V.; Padmaja, S.; Au, V.; Madison S. A. *J. Chem. Soc., Perkin Trans. 2* **1999**, 1219−223.

(40) Padmaja, S.; Madison, S. A. *J. Phys. Org. Chem*. **1999**, *12*, 221−226.

(41) Bagyo, A. N. M.; Arai, H.; Miyata, T. *Appl. Radiat. Isotop*. **1997**, *48* (2), 175−181.

(42) Panajkar, M. S.; Mohan, H. *Indian J. Chem*. **1993**, *32A*, 25−27.

(43) Destaillats, H.; Colussi, A. J.; Joseph, J. M.; Hoffmann, R. *J. Phys. Chem. A* **2000**, *104*, 8930−8935.

(44) Joseph, J. M.; Destaillats, H.; Hung, H.; Hoffmann, M. R. *J. Phys. Chem. A* **2000**, *104*, 301−307.

(45) Naffrechoux, E.; Chanoux, S.; Petrier, C.; Suptil, J. *Ultrasonics Sonochem.* **2000**, *7*, 255−259.

(46) Richter, H. W. In *Photochemistry and Radiation Chemistry*; Wishart, J. F., Nocera, D. G., Eds.; Oxford University Press: New York, 1998.

(47) Leffler, J. E. In *An Introduction to Free Radicals*; Wiley-Interscience: New York, 1993.

(48) Von Sonntag, C.; Dowideit, P.; Fang, X.; Mertens, R.; Pan, X.; Schuchmann, M. N.; Schuchmann, H. P. *Water Sci. Technol*. **1997**, *35* (4), 9−15.

(49) Zhan, H.; Chen, K.; Tian, H. *Dyes Pigments* **1998**, *37* (3), 241−247.

(50) Oakes, J.; Gratton, P. *J. Chem. Soc., Perkin Trans. 2* **1998**, 1857−1864.

(51) Parr, R. G.; Yang, W. *Annu. Rev. Phys. Chem*. **1995**, *46*, 701.

(52) Geerlings, P.; De Proft, F.; Langenaeker, W. Density functional Theory: A Source of chemical concepts and a Cost-Effective Methodology for Their Calculation. In *Advances in Quantum Chemistry*: *Density functional Theory*; Seminario, J. M., Ed.; Academic Press: New York, 1999; Vol 33, p 303.

(53) Lim, M. H.; Worthington, S. E.; Dulles, F. J.; Cramer, C. J. Density Functional Calculations of Radicals and Diradicals. In *Density-Functional Methods in Chemistry*; Laird, B. B., Ross, R. B., Ziegler, T., Eds.; ACS Symposium Series, Volume 629; American Chemical Society: Washington, DC, 1996; p 402.

(54) Bally, T.; Borden, W. T. Calculations on Open-Shell Molecules: A Beginner's Guide. In *Reviews in Computational Chemistry*; Lipkowitz, K. B., Boyd, D. B., Eds.; Wiley-VCH, John Wiley and Sons: New York, 1999; Vol. 13, p 1.

(55) Parr, R. G.; Yang, W. *Density-Functional Theory of Atoms and Molecules*; Oxford University Press: New York, 1989.

(56) Jensen, F. *Introduction to Computational Chemistry*; John Wiley and Sons Ltd.: Chichester, U.K., 1999.

(57) Wong, M. W.; Radom, L. *J. Phys. Chem. A* **1998**, *102*, 2237−2245.

(58) Sekusak, S.; Liedl, K. R.; Sabljic, A. *J. Phys. Chem. A* **1998**, *102*, 1583−1594.

(59) Llano, J.; Erikkson, L. A. *J Phys. Chem B* **1999**, *103*, 5598−5607.

(60) Parr, R. G.; Yang, W. *J. Am. Chem. Soc*. **1984**, *106*, 4049−4050.

(61) Yang, W.; Mortier, W. J. *J. Am. Chem. Soc.* **1986**, *108*, 5708-

(62) Pearson, R. G. *J. Chem. Educ.* **1987**, *64*, 561.

(63) Lee, C.; Yang, W.; Parr, R. G. *J. Mol. Struct. (THEOCHEM)* **1988**, *163*, 305−313.

(64) Gazquez, J. L.; Mendez, F. *J. Phys. Chem*. **1994**, *98*, 4591−1994.

(65) De Proft, F.; Martin, J. M. L.; Geerlings, P. *Chem. Phys. Lett*. **1996**, *256*, 400−408.

(66) Misra, G. P.; Sannigrahi, A. B. *J. Mol. Struc (THEOCHEM)* **1996**, *361*, 63−68.

(67) Gazquez, J. L. *J. Phys. Chem. A* **1997**, *101*, 9464−9469.

(68) Chandra, A. K.; Nguyen, M. T. *J. Chem. Soc., Perkin Trans. 2* **1997**, 1415−1417.

(69) Roy, R. K.; Krishnamurti, S.; Geerlings, P.; Pal, S. *J. Phys. Chem. A* **1998**, *102*, 3746−3755.
(70) Bonn, G.; De Proft, F.; Langenaeker, W.; Geerlings, P. *Chem. Phys. Lett.* **1998**, *295*, 122−128.
(71) Gillardoni, F.; Weber, J.; Chermette, H.; Ward, T. R. *J Phys. Chem. A* **1998**, *102*, 3607−3613.
(72) Balawender, R.; Komorowski, L. J. *Chem. Phys.* **1998**, *109*, 5203−5211.
(73) Roy, R. K.; Choho, K.; De Proft, F.; Geerlings, P. *J. Phys. Org. Chem.* **1999**, *12*, 503−509.
(74) Mineva, T.; Russo, N.; Sicilia, E.; Toscano, M. *Theor. Chem. Acc* **1999**, *101*, 338-
(75) Roy, R. K.; Pal, S.; Hirao, K. J. *Chem. Phys.* **1999**, *110*, 8236−8245.
(76) Chermette, H. *J. Comput. Chem.* **1999**, *20*, 129−154.
(77) Sivanesan, D.; Amutha, R.; Subramanian, V.; Nair, B. U.; Ramasami, T. *Chem. Phys. Lett.* **1999**, *308*, 223−228.
(78) Pearson, R. G. *J. Chem. Educ.* **1999**, *76*, 267−275.
(79) Geerlings, P.; De Proft, F. *Int. J. Quantum Chem.* **2000**, *80*, 227−235.
(80) Roy, R. K.; Hirao, K. *J. Chem. Phys.* **2000**, *113*, 1372-
(81) Krishnamurty, S.; Pal, S. *J. Phys. Chem. A* **2000**, *104*, 7639−7645.
(82) Korchowiec, J. *Comput. Chem.* **2000**, *24*, 259−262.
(83) Kar, T.; Sannigrahi, A. B. *Indian J. Chem.* **2000**, Vol39 A, 68−74.
(84) Chandra, A. K.; Uchimaru, T.; Sugie, M.; Sekiya, A. *Chem. Phys. Lett.* **2000**, *318*, 69−74.
(85) Cruz, J.; Martinez, L. M. R.; Salcedo, R.; Castro, M. *Int. J. Quantum Chem.* **2001**, *85*, 546−556.
(86) Pilepic, V.; Ursic, S. *J. Mol. Struct. (THEOCHEM)* **2001**, *538*, 41−49.
(87) Mitnik, D. G., Lucero, A. M. *J. Mol. Struct. (THEOCHEM)* **2001**, *535*, 39−47.
(88) Nguyen, L. T.; De Proft, F.; Chandra, A. K.; Uchimaru, T.; Nguyen, M. T.; Geerlings, P. *J. Org. Chem.* **2001**, *66*, 6096−6103.
(89) Balawender, R.; Safi, B.; Geerlings, P. *J. Phys. Chem. A* **2001**, *105*, 6703−6710.
(90) Chandra, A. K.; Uchimaru, T. *Chem. Phys. Lett.* **2001**, *334*, 200−206.
(91) Roy, R. K.; Hirao, K.; Krishnamurty, S.; Pal, S. *J. Chem. Phys.* **2001**, *115*, 2901−2907.
(92) De Proft, F.; Geerlings, P. *Chem. Rev.* **2001**, *101*, 1451−1464.
(93) Fuentealba, P.; Pérez, P.; Contreras, R. *J. Chem. Phys.* **2001**, *113*, 2544−2551.
(94) Frisch, M. J.; Trucks, G. W.; Schlegel, H. B.; Scuseria, G. E.; Robb, M. A.; Cheeseman, J. R.; Zakrzewski, V. G.; Montgomery, J. A., Jr.; Stratmann, R. E.; Burant, J. C.; Dapprich, S.; Millam, J. M.; Daniels, A. D.; Kudin, K. N.; Strain, M. C.; Farkas, O.; Tomasi, J.; Barone, V.; Cossi, M.; Cammi, R.; Mennucci, B.; Pomelli, C.; Adamo, C.; Clifford, S.; Ochterski, J.; Petersson, G. A.; Ayala, P. Y.; Cui, Q.; Morokuma, K.; Malick, D. K.; Rabuck, A. D.; Raghavachari, K.; Foresman, J. B.; Cioslowski, J.; Ortiz, J. V.; Stefanov, B. B.; Liu, G.; Liashenko, A.; Piskorz, P.; Komaromi, I.; Gomperts, R.; Martin, R. L.; Fox, D. J.; Keith, T.; Al-Laham, M. A.; Peng, C. Y.; Nanayakkara, A.; Gonzalez, C.; Challacombe, M.; Gill, P. M. W.; Johnson, B. G.; Chen, W.; Wong, M. W.; Andres, J. L.; Head-Gordon, M.; Replogle, E. S.; Pople, J. A. *Gaussian 98*, revision A.7; Gaussian, Inc.: Pittsburgh, PA, 1998.
(95) Tomasi, J.; Mennucci, B.; Cancés, E. *J. Mol. Struct. (THEOCHEM)* **1999**, *464*, 211−226.
(96) Biegler-König, F. *J. Comput. Chem.* **2000**, *21*, 1040−1048. Bielkgler-König, F.; Schönbohm, J.; Bayles, D. *J. Comput. Chem.* **2001**, *22*, 545−559.
(97) Bader, R. F. W. Atoms in Molecules: A Quantum Theory. *International Series of Monographs on Chemistry*; Clarendon Press: Oxford, 1995; Vol. 22, pp 1−438.
(98) Espinosa, E.; Molins, E. *J. Chem. Phys.* **2000**, *113*, 5686−5694.
(99) Patai, S. *The Chemistry of the Hydrazo, Azo, and Azoxy Groups*; John Wiley: New York, 1975.
(100) Safi, B.; Choho, K.; De Proft, F.; Geerlings, P. *J. Phys. Chem. A* **1998**, *102*, 5253−5259.